ACS OMEGA

http://pubs.acs.org/journal/acsodf
Article

High-Efficiency Adsorption of Cr(VI) and Mn(VII) from Wastewater by a Two-Dimensional Copper-Based Metal−Organic Framework

Yongmou Zeng, Xia Li, Yuhuan Chen, and Shixiong Li*

Cite This: *ACS Omega* 2023, 8, 36978−36985
Read Online

ACCESS | Metrics & More | Article Recommendations | Supporting Information

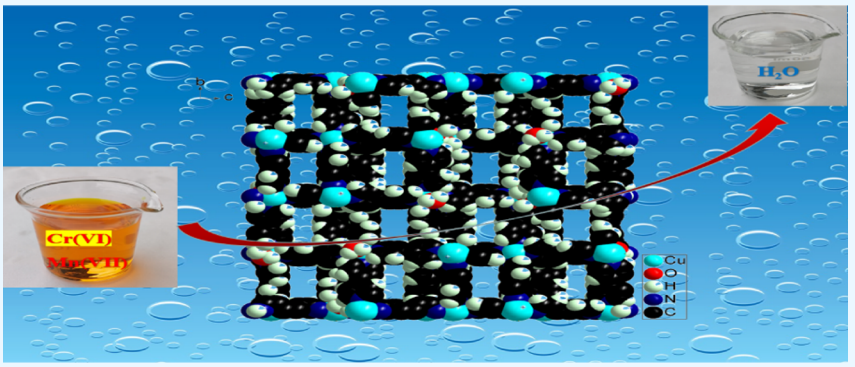

ABSTRACT: Cr(VI) and Mn(VII) in industrial wastewater have certain toxicity, and they pose a threat to the environment and human health and safety. Metal−organic frameworks (MOFs) usually have rich adsorption sites and a large specific surface area. They can effectively adsorb Cr(VI) and Mn(VII) from wastewater. In this paper, a two-dimensional copper-based metal−organic framework, $\{[Cu\cdot(4,4'\text{-bpy})_2\cdot(H_2O)]\cdot 2(NO_3)\cdot 6(H_2O)\cdot(CH_3OH)\}_n$ (**1**), is synthesized by hydrothermal synthesis. The structure of **1** is characterized by Fourier transform infrared (IR) spectroscopy, single-crystal X-ray diffraction, element analysis, and X-ray photoelectron spectroscopy (XPS). The results showed that **1** had a two-dimensional network structure, and the specific surface area of the nanostructure was 67.63 m^2/g. The nanostructure of **1** could efficiently adsorb Cr(VI) and Mn(VII) from wastewater. The adsorption properties of Cr(VI) and Mn (VII) of **1** showed that the optimal concentration of both adsorbents was 0.2 g/L. It has good adsorption performance in the pH range 4−8. The adsorption performance is the best when pH is 7, which can reach 145 and 83 mg/g, respectively.

1. INTRODUCTION

Industrial wastewater pollution sources refer to wastewater and waste liquid generated in the process of industrial production.[1] Industrial wastewater has the characteristics of complex components, multiple types, and high concentrations of pollutants. They mainly include ammonia nitrogen, petroleum, volatile phenol, heavy metals, and other harmful and toxic substances.[2−4] The grinding process of artificial diamond precision cutting tools often generates a large amount of heavy metal wastewater. These heavy metal ions mainly include Cu(II), Fe(III), Hg(II), Cr(VI), and Mn(VII).[5] They pose a threat to the environment and human health and safety. At present, there are many methods to remove high-valence heavy metal ions, such as chemical precipitation,[6] photocatalytic reduction,[7] electrochemical reduction,[8] and adsorption.[9] In the field of wastewater treatment, adsorption is a transfer process between two liquid−solid phases. It is a process that uses the surface of the porous solid adsorbent to adsorb one or more pollutants in wastewater to achieve wastewater purification. There are many kinds of adsorbents,[10−12] but activated carbon is widely used in industrial wastewater treatment. The activated carbon is generally processed into a powder or granule. Powdered activated carbon has a strong adsorption capacity, easy preparation, and low price, but it is difficult to regenerate and cannot be reused generally. Therefore, more adsorbents (zeolite, diatomite, molecular brush, graphene, and complex) have been developed to treat industrial wastewater. Coordination polymers[13] usually have rich adsorption sites, which can effectively adsorb Cr(VI) and Mn(VII).[14−16]

Finding efficient and sustainable methods to remove metal ions is an important research field in current environmental and water pollution issues. Some coordination polymers have shown great potential applications in magnetism,[17] fluorescence,[18] photocatalytic degradation,[19] catalytic synthesis,[20] and bio-

Received: June 13, 2023
Accepted: September 15, 2023
Published: September 29, 2023

https://doi.org/10.1021/acsomega.3c04177
ACS Omega 2023, 8, 36978−36985

logical activity.[21] Copper-based metal−organic frameworks (Cu-MOFs) are gradually becoming a new trend for metal ion adsorption and removal.[22−24] This is mainly because Cu-MOFs have advantages of high adsorption capacity, high selectivity, renewability, and functionalization modification. First, they have multiple active adsorption sites and can efficiently adsorb metal ions through mechanisms such as electrostatic interactions and coordination exchange. Second, they can be regenerated and recycled through methods such as pyrolysis, making them sustainable metal ion adsorption materials. They can reduce the cost of adsorption and removal of heavy metal ions. Finally, by the introduction of functional groups onto Cu-MOFs, their interactions with specific metal ions can be increased, thereby improving adsorption capacity and selectivity. For example, introducing functional groups such as nitrogen and phosphorus[22] can enhance the adsorption capacity of heavy metal ions. Especially, these two-dimensional Cu-MOFs composed of cationic frameworks and counteranions exhibited excellent performance in adsorbing Cr(VI).[9] This was because Cr(VI) exhibited a certain electrostatic attraction with the cationic framework, which facilitated adsorption. Therefore, synthesizing MOFs composed of cationic frameworks and counteranions will effectively adsorb Cr(VI) and Mn(VII).

In this paper, a copper-based coordination polymer, $\{[Cu\cdot(4,4'\text{-bpy})_2\cdot(H_2O)]\cdot 2(NO_3)\cdot 6(H_2O)\cdot(CH_3OH)\}_n$ (**1**), is successfully synthesized by the 4,4′-bpy and $Cu(NO_3)_2\cdot 3H_2O$ as raw materials. The structure of **1** is characterized by IR, single-crystal X-ray diffraction, element analysis, and XPS. The effects of adsorbent concentration, pH, and temperature on the adsorption of Cr(VI) and Mn(VII) are investigated. The results showed that **1** had good adsorption performance in the pH range 4−8. The adsorption performance was the best when pH is 7, which could reach 145 mg/g and 83 mg/g, respectively.

2. EXPERIMENTAL SECTION

2.1. Instruments and Reagents. The IR spectra were recorded on KBr pellets with a Nicolet 5DX FT-IR spectrometer. The elemental analysis (carbon, hydrogen, and nitrogen) was performed with a PerkinElmer 240 elemental analyzer. The X-ray crystallography was collected on a Bruker Apex CCD area-detector diffractometer. The XPS measurements were performed on a Kratos Axis Ultra DLD system with a base pressure of 10^{-9} Torr. The X-ray powder diffraction (XRD) was performed using a Rigaku D/max 2500 X-ray diffractometer with Cu Kα radiation (λ = 0.15604 nm); the tube voltage was 40 kV, the tube current was 150 mA, a graphite monochromator was used, and 2θ was 5°−50°. The scanning electron microscopy (SEM) was performed by using the Hitachi S-4800 under the following conditions: Mag.: 1 KX; Signal A: VPSE, and EHT: 20 kV. The transmission electron microscopy (TEM) images and energy-dispersive spectroscopy (EDX) were taken with a JEOL ARM200F microscope (JEOL, Tokyo, Japan). The surface area was determined using the BET technique; the apparatus (AUTO CHEMII 2920) was employed to determine the surface area by using N_2 as the probe gas; nonlinear least-squares method was used to fit the data and draw a graph using Origin 8.5. The thermal stability was tested on a Pyris Diamond TG-DTG Analyzer. The concentrations of Cr(VI) and Mn(VII) were analyzed using a UV-2601 UV−vis spectrophotometer produced by Beijing Ruili Analytical Instrument Co., Ltd.

The chemical reagents used in the experiment, such as 4,4′-bpy, $Cu(NO_3)_2\cdot 3H_2O$, $K_2Cr_2O_7$, $KMnO_4$, and methanol, are analytically pure reagents produced by Energy Chemical Co., Ltd. (Shanghai, China). The pure water used in the experiment was prepared by reverse osmosis in the laboratory.

2.2. Synthesis of $\{[Cu\cdot(4,4'\text{-bpy})_2\cdot(H_2O)]\cdot 2(NO_3)\cdot 6(H_2O)\cdot(CH_3OH)\}_n$ (1). A mixture of $Cu(NO_3)_2\cdot 3H_2O$ (0.0241 g, 0.1 mmol) and 4,4′-bpy (0.0610 g, 0.2 mmol) were mixed in 10 mL of water and 10 mL of anhydrous methanol. Stir for 2 h at room temperature. After the reaction is over, filter and collect the filtrate in a 50 mL beaker. The filtrate volatilized naturally for 7 days to obtain blue blocky crystals. The yield is about 95% (based on Cu^{2+}). Elemental analyses are as follows: calcd (%) for ($C_{21}H_{32}CuN_6O_{13}$): C 39.39, N 13.10, H 5.02; Found: C 39.37, N 13.12, H 5.00. IR data for (KBr, cm^{-1}): 3416 (m), 3049 (w), 2918 (w), 2426 (w), 1613 (m), 1534 (m), 1383 (s), 1226 (w), 1075 (w), 813 (s), 728 (w), 636 (w), and 452 (w).

2.3. Single-Crystal X-ray Diffraction. A single crystal with a size of approximately 0.14 × 0.12 × 0.10 mm^3 in **1** was used for structural test analysis on a single-crystal X-ray diffractometer. Use a Bruker APEX-IICCD single-crystal diffractometer to collect **1** single-crystal data. The intensity data of **1** were collected on a Bruker SMART APEX IICCD diffractometer (Mo Kα radiation, λ = 0.71073 Å) at room temperature. The test conditions are as follows: Mo−Kα radiation is a diffractive light source (λ = 0.071073 nm); T = 180(2) K; and the data collection ranges are $-20 \le h \le 15$, $-52 \le k \le 52$, and $-52 \le l \le 55$. A total of 7866 reflections were collected during the test, of which the only reflection was 3609, and $R_{(int)}$ = 0.079. After the **1** single-crystal receipt is collected, the Olex2 software[25] is used to analyze its structure, hydrogenate, and refine it. The parameters of **1** crystals are listed in Table S1, and some of the bond lengths and bond angles are listed in Table S2. CCDC: 2233261.

2.4. Adsorption Experiment. The experimental parameters of polymer **1** adsorption of Cr(VI) and Mn(VII) are as follows: the dosage of **1** is 0.0010−0.0050 g; the concentrations of Cr(VI) and Mn(VII) are 50 mg/L and 35 mg/g, respectively; the pH of the solution is 4−8; and the dosages of Cr(VI) and Mn(VII) are 100 mL. During the experiment, 0.0010 g of **1** was added into a 250 mL beaker with a circulating water system, and then 100 mL of Cr(VI) and Mn(VII) with a concentration of 50 mg/L were added into the beaker, put in a magnetic stirrer, and placed it in parallel on the magnetic stirrer. After stirring and adsorbing for 10, 20, 30, 40, and 50 min at a temperature of 25−45 °C, 10 mL of the mixed solution was drawn with a 10 mL syringe, a 0.45 um filter was installed, and the collected filtrate was put into a cuvette. The absorbance was measured with an ultraviolet−visible spectrophotometer. The adsorption performance was evaluated by the change of Cr(VI) and Mn(VII) concentrations before and after the reaction. The adsorption rate was calculated as follows

$$R = \left(1 - \frac{C_t}{C_0}\right) \times 100\%$$

where R is the adsorption rate (%). For the adsorption experiment, C_0 and C_t are the initial concentration and the concentration at t, respectively ($mg\cdot L^{-1}$).

3. RESULTS AND DISCUSSION

3.1. Structure of 1. *3.1.1. IR.* IR can be used to analyze the functional groups contained in materials. Therefore, the IR of 4,4′- bpy and **1** w ere measured at room temperature. The test results (Figure S1) showed that the peaks at 3049, 2918, and 1649 cm^{-1} were the infrared absorption peaks of the −C═N

https://doi.org/10.1021/acsomega.3c04177
ACS Omega 2023, 8, 36978−36985

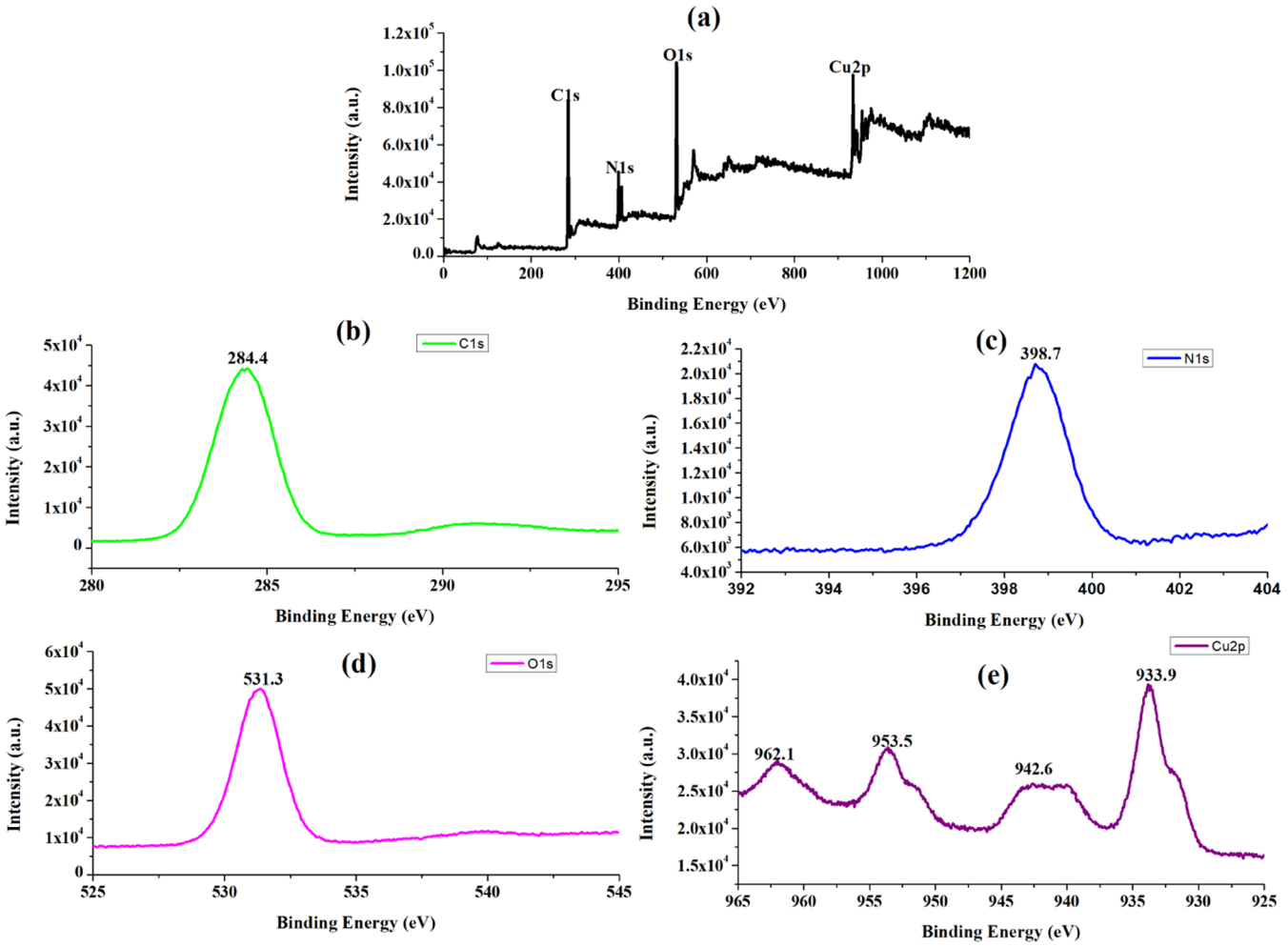

Figure 1. XPS of **1**: (a) full spectrum; (b) C(1s); (c) N(1s); (d) O(1s); and (e)Cu(2p).

bond. Among them, the absorption peaks at 3049 and 2918 cm^{-1} are the twisted vibrations of the −C═N double bond. The absorption peak at 1649 cm^{-1} is caused by a resonant vibration of −C═N. The absorption peak at 3416 cm^{-1} belongs to the −OH stretching vibration peak of H_2O. The absorption at 1613 cm^{-1} is the skeleton stretching vibration of the benzene ring.

3.1.2. XPS. XPS can be used to determine the composition of materials and the distribution of valence states of elements. The XPS of **1** (Figure 1) shows that it is composed of Cu, C, N, O, and other elements (Figure 1a). The peak of C(1s) appears at 284.4 eV (Figure 1b). The peak of N(1s) appears at 398.7 eV (Figure 1c). The peak of O (1s) appears at 531.3 eV (Figure 1d). The peaks of Cu (2p) appear at 962.1 953.5, 942.6, and 933.9 eV (Figure 1e), and these peaks are all from Cu (II). Therefore, the valence state of Cu ion in **1** is +2.[9]

3.1.3. Single-Crystal X-ray Diffraction. Single-crystal X-ray diffraction shows that the molecular structure of **1** is $\{[Cu\cdot(4,4'\text{-bpy})_2\cdot(H_2O)]\cdot 2(NO_3)\cdot 6(H_2O)\cdot(CH_3OH)\}_n$. It belongs to the orthorhombic crystal system, *Fddd* space group, with a = 1.45149 (12) nm, b = 4.1897 (4) nm, c = 4.1989 (4) nm, $\alpha = \beta = \gamma = 90°$, and V = 25.535(4) nm^3. **1** belongs to the inorganic coordination polymer. It is composed of $[Cu\cdot(4,4'\text{-bpy})_2\cdot(H_2O)]^{2+}$ framework and counterbalance NO_3^- anion. In $[Cu\cdot(4,4'\text{-bpy})_2\cdot(H_2O)]^{2+}$, the central Cu(II) is coordinated with four N atoms (N(1), N(2), N(3A), and N(4) are from 4,4′-bipyridine molecules) and one O atom (O(1) is from water molecule) (Figure 2a), respectively. Therefore, Cu(II) in **1** is pentacoordinated. In **1**, Cu(1)−N(1) = 2.026(4) Å, Cu(1)−N(2) = 2.037(4) Å, Cu(1)−N(3) = 2.025(4) Å, Cu(1)-N(4A) = 2.042(4) Å, and Cu(1)−O(1) = 2.404(4) Å. The bond length of Cu−O is longer than that of Cu−N, which may be due to the influence of the Jahn−Teller effect. The N atoms on 4,4′-bpy molecules in **1** coordinate with adjacent Cu(II) (Figure 2b), respectively. It is very interesting that the 2D layers are not stacked but are interconnected in **1** (Figure 2c). This is due to the different orientations of 4,4′-bpy in **1** (Figure 2b). In this way, a 2D surface with certain porosity is formed (Figure 2d).

3.1.4. SEM, TEM, and EDS Mapping. **1** (Figure 3a) is a blur material. Scanning electron microscopy (SEM) can be used to observe the morphology and size of nanomaterials. The SEM test of the nanocrystal of **1** (Figure 3b) shows that its morphology is basically rectangular. The average particle diameter of nanomaterials is about 500 mm. The nanostructure of **1** was confirmed by STEM-EDS elemental mapping analysis. The STEM results showed that its size was about 50 nm (Figure 3c−3e), and EDS mapping showed that it was composed of Cu, C, N, and O elements (Figure 3f−3i).

3.2. N_2 Adsorption/Desorption Isotherm. As 4,4′-bipyridine is a bridging ligand, it can often be introduced into the complexes to obtain coordination polymers with certain pores. The N_2 adsorption/desorption isotherm of **1** (Figure S2) shows that it belongs to a typical s-type adsorption isotherm.

https://doi.org/10.1021/acsomega.3c04177
ACS Omega 2023, 8, 36978−36985

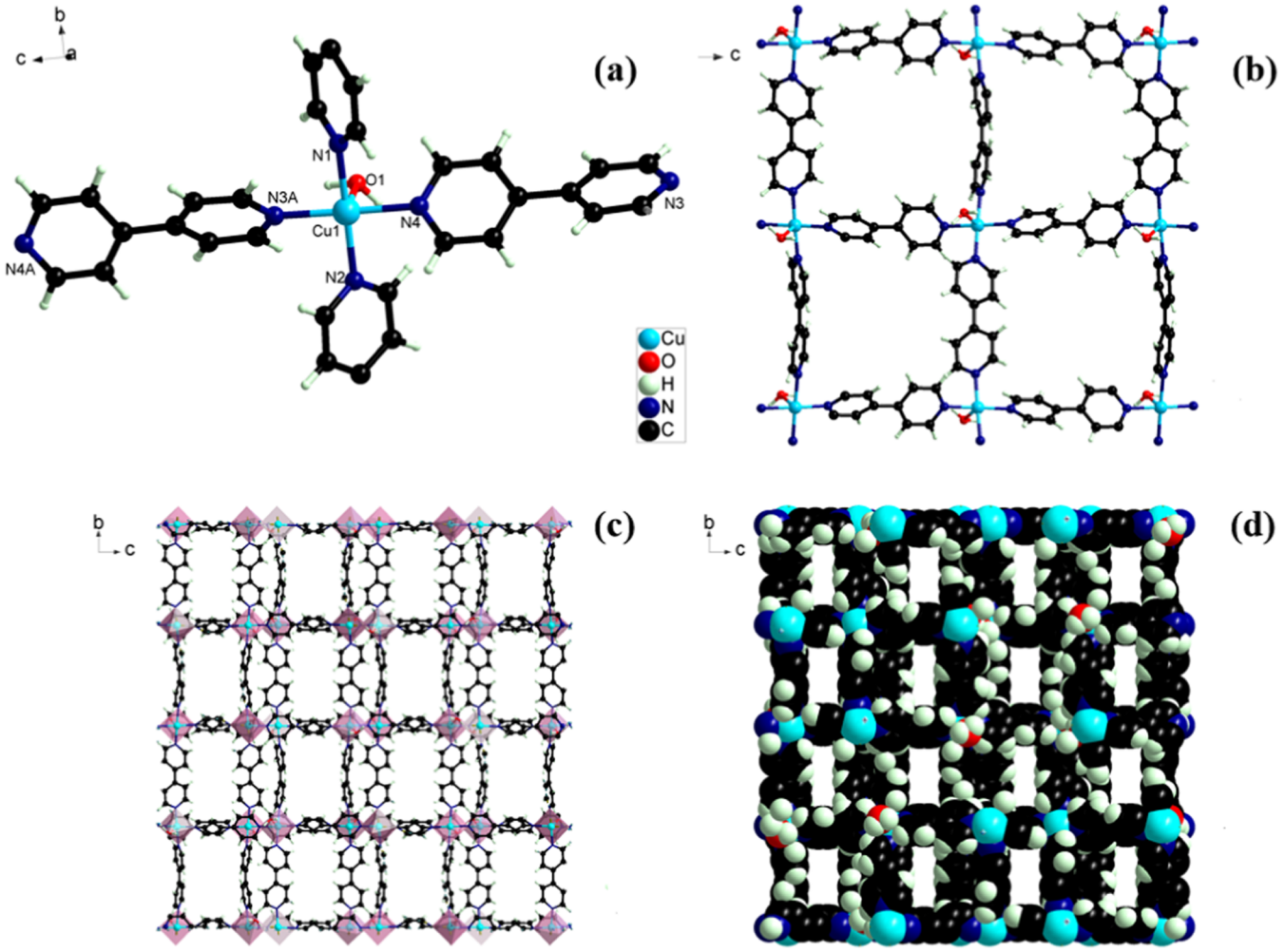

Figure 2. (a) Coordination mode of **1**; (b) 4,4′- bipyridine-bridged Cu (II); (c) two-dimensional structure formed by bridging Cu(II) with 4,4′-bipyridine; and (d) 2D stacked structure.

The BET-specific surface area (Table 1) of **1** is 67.63 m^2/g, and the Langmuir-specific surface area is 130.5 m^2/g. Its pore volume is 0.24 cm^3/g, and the pore diameter of adsorption and desorption is 26.27 nm (Figure S3). The Langmuir surface area is too high compared with the BET one, which should be the calculation of the BET-specific surface area based on multi-molecular layer adsorption.

3.3. Thermogravimetric Analysis. **1** was analyzed by thermogravimetry in the range of 30−1000 °C when N_2 is the protective gas and the heating rate is 5 °C/min. The result (Figure S4) shows the weight loss of 15.21% of **1** in the range of 30−153 °C, which is mainly due to the loss of water molecules and methanol molecules. In the range of 154−321 °C, the weight loss is 70.95%, which is mainly due to the loss of 4,4′-bpy molecules and NO_3^-. Finally, 13.84% of metal oxides is left (theoretically, 12.4% of CuO).

3.4. Adsorption of Cr(VI) and Mn(VII). *3.4.1. Effect of Adsorbent Dosage on Adsorption.* At 25 °C, a certain amount (0.0100−0.0500 g) of **1** adsorbent was added to the $Cr_2O_7^{2-}$ and MnO_4^- solution with pH 7 to study the effect of adsorbent dosage on the adsorption of Cr(VI) and Mn(VII). The experimental results (Figure 4) show that **1** can reach adsorption equilibrium after 40 min of adsorption. It can be seen from Figure 4a that 0.0100 g of **1** can reach the adsorption equilibrium after 40 min of adsorption. It can adsorb 27% Cr(VI), and the adsorption amount is 135 mg/g; 0.0200−0.0500 g of **1** can reach the adsorption equilibrium after 40 min of adsorption Cr(VI). It can adsorb 58, 85, 91, and 95% Cr(VI), respectively. The adsorption amounts are 145, 140, 114, and 95 mg/g, respectively.

Similarly, **1** can reach adsorption equilibrium after adsorbing Mn(VII) for 40 min (Figure 4b). 0.0100−0.0500 g of **1** can adsorb 23, 48, 65, 80, and 87% Mn(VII), respectively. The adsorption amounts are 78, 83, 75, 69, and 60 mg/g, respectively. It can be seen (Figure 4c,d) that the adsorption capacity of the adsorbent does not increase with the increase in the adsorbent dosage, but there is an optimal adsorption capacity. The optimal adsorbent dosage of Cr(VI) (Figure 4c) and Mn(VII) (Figure 4d) adsorbed by **1** is 0.0200 g, that is, when the adsorbent concentration is 0.2000 g/L, the adsorption capacity is the best, which can reach 145 and 83 mg/g, respectively. Although the maximum adsorption capacity of **1** can be as high as 145 and 83 mg/g, the adsorption capacity is better than most adsorbents.[26] But, it is inferior to the maximum adsorption capacity of 372.6 mg/g (Table 2) reported in the literature.[27] The amounts of Cr(VI) and Mn(VII) adsorbed are obviously better than those of most adsorbents, which may be due to the structure of **1**. **1** has a cationic structural framework $[Cu{\cdot}(4,4'\text{-bpy})_2{\cdot}(H_2O)]^{2+}$. In addition to the adsorption of Cr(VI) and Mn(VII) by pores and hydrogen bonds, **1** can also

https://doi.org/10.1021/acsomega.3c04177
ACS Omega 2023, 8, 36978−36985

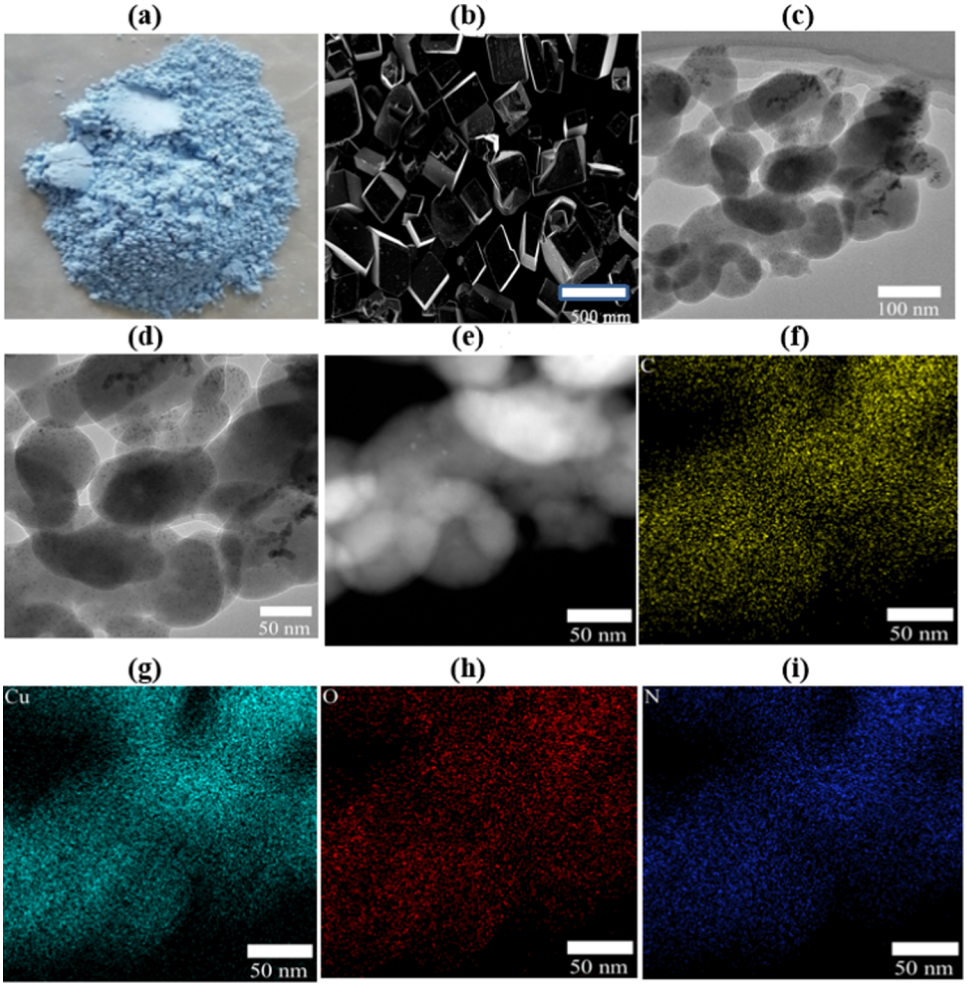

Figure 3. (a) The color of **1**; (b) SEM of **1**; (c)−(e) STEM of nanostructure of **1**; and (f)−(i) EDS mapping of **1**.

Table 1. Characterization and Analysis Results of N_2 Adsorption/Desorption Isotherms of 1

parameter	value	parameter	value
single-point surface area	44.71 m^2/g	BET surface area	67.63 m^2/g
Langmuir surface area	130.52 m^2/g	t-Plot external surface area	98.32 m^2/g
pore volume	0.24 cm^3/g	pore size	26.27 nm

be adsorbed by charge attraction. The rich adsorption capacity makes it able to effectively adsorb Cr(VI) and Mn(VII). So the amount of Cr(VI) and Mn(VII) adsorbed by **1** can reach 145 and 83 mg/g.

3.4.2. Influence of pH on Adsorption. At 25 °C, 0.0200 g of adsorbent was added to different pH solutions (4−8) to study the effect of pH on the adsorption of Cr(VI) and Mn(VII). The experimental results (Figure 5a) show that Cr(VI) can be adsorbed by **1** at pH 4, 5, 6, 7, and 8, and the adsorption equilibrium can be reached after 40 min. The removal rates of Cr(VI) are 49, 52, 55, 58, and 53%, respectively. The adsorption amounts are 122.5, 130, 137.5, 145, and 132.5 mg/g, respectively. It can be seen that the optimal pH in the solution is 7, and the adsorption capacity is 145 mg/g.

Similarly, the **1** adsorbs Mn(VII) can reach adsorption equilibrium after 40 min under different pH (4, 5, 6, 7, and 8) (Figure 5b). Under different pH conditions, the removal rates of Mn(VII) are 39, 42, 45, 48, and 44%, respectively. The adsorption amounts are 68.25, 73.5, 78.75, 83, and 77 mg/g, respectively. It can be seen that the optimal pH in the solution is 7, and the adsorption capacity is 83 mg/g. From the experimental results of pH affecting the adsorption of Cr(VI) and Mn(VII) on **1**, it can be found that pH has little effect on the adsorption of Cr(VI) and Mn(VII) on **1**. This shows that the adsorption of Cr(VI) and Mn(VII) by **1** has broad pH adaptability.

3.4.3. Influence of Temperature on the Adsorption of Cr(VI) and Mn(VII). Add 0.0200 g of **1** to the $Cr_2O_7^{2-}$ and MnO_4^- solution with pH 7 to explore the effect of temperature (25−45 °C) on the adsorption of Cr(VI) and Mn(VII). The experimental results show that the adsorption equilibrium can be reached at 25, 30, 35, 40, and 45 °C after 40 min (Figure 6a). The removal rates of Cr(VI) are 58, 60, 63, 65, and 64%, respectively, and the adsorption capacities are 145 150, 157.5, 162.5, and 160 mg/g, respectively. It can be seen that the optimum temperature for **1** to adsorb Cr(VI) is 40 °C, and its maximum adsorption capacity is 162.5 mg/g. At the same temperature, the removal rates of Mn(VII) adsorbed by **1** (Figure 6b) are 48, 50, 45, 40, and 46%, respectively. The adsorption capacities are 83 87.5, 78.75, 79, and 80.5 mg/g, respectively. Therefore, the optimal adsorption temperature for Mn(VII) adsorption by **1** is 30 °C, and the maximum adsorption amount at this temperature is 87.5 mg/g.

https://doi.org/10.1021/acsomega.3c04177
ACS Omega 2023, 8, 36978−36985

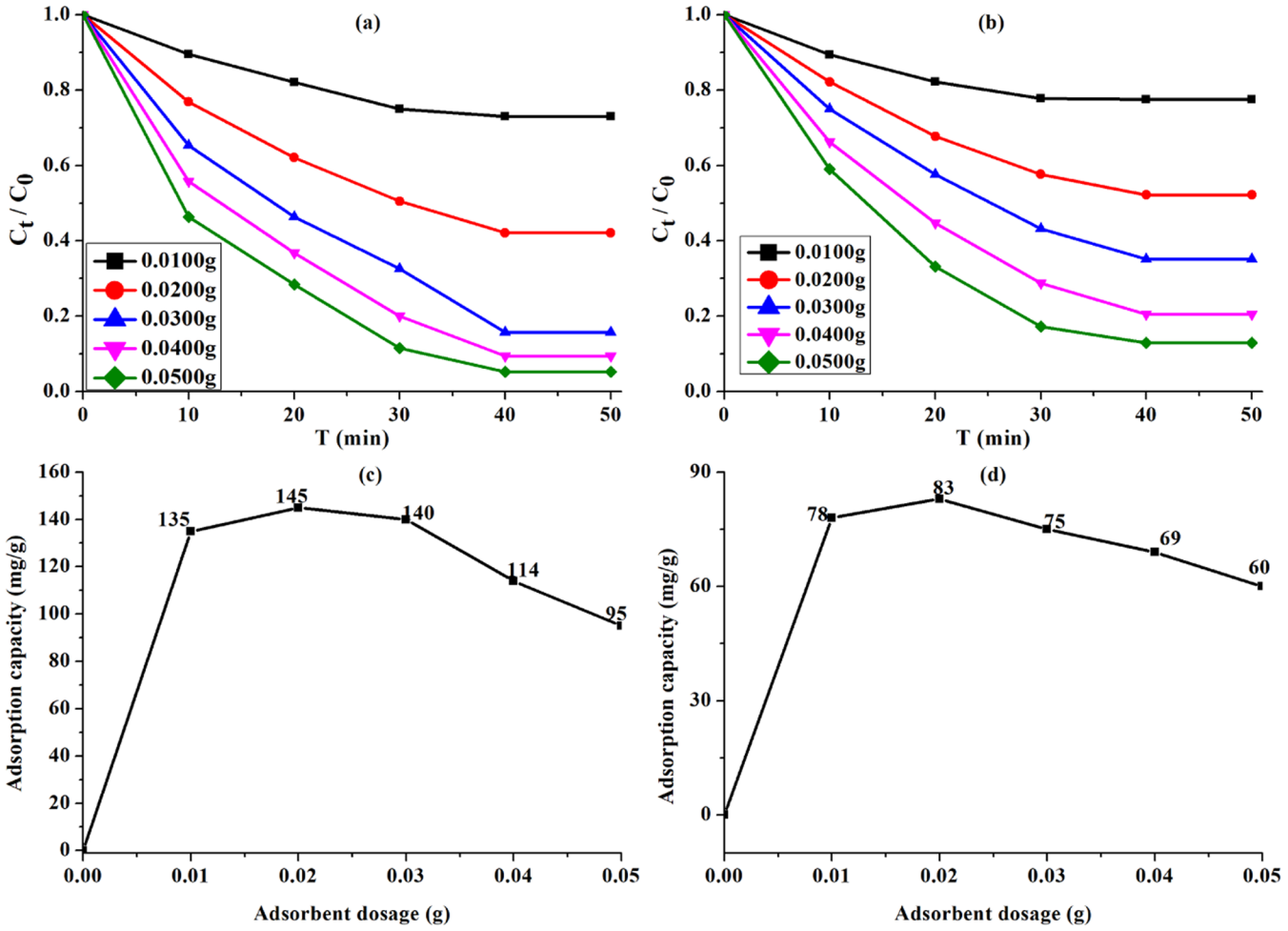

Figure 4. (a, b) Influence of **1** adsorbent dosage on the adsorption of Cr(VI) and Mn(VII); (c, d) the maximum adsorption capacity of Cr(VI) and Mn(VII).

Table 2. Cr(VI) Adsorption Performance of Some Reported MOFs

MOF	adsorbate	adsorption capacity (mg/g)	ref
ABT-$(ClO_4)_2$	Cr(VI)	271	26
ZJU	Cr(VI)	245	26
MONT-1	Cr(VI)	211.8	26
TMU-30	Cr(VI)	145	26
NiCo-LDH	Cr(VI)	99.9	26
UPC-50	Cr(VI)	56.8	26
UIO-66-NH_2	Cr(VI)	32.4	26
PAN/chitosan/UiO-66-NH_2	Cr(VI)	372.6	27

3.5. Regeneration and Recycling Experiment of Adsorbent. The regeneration and adsorption efficiency of adsorbents is one of the main reasons affecting their application. Therefore, the adsorbent is collected by a high-speed centrifuge of 10,000 rpm/min after the **1** adsorbed of Cr(VI) and Mn(II). Then, add 0.001 mol/L HNO_3 to the adsorbent and mix ultrasonically for 30 min. Centrifugally collect the adsorbent, wash it with deionized water and anhydrous methanol three times, respectively, and finally dry the collected adsorbent in an oven at 80 °C for 12 h. The structure of the adsorbent after drying (the recovery rate was approximately 99%) was tested by X-ray powder diffraction.

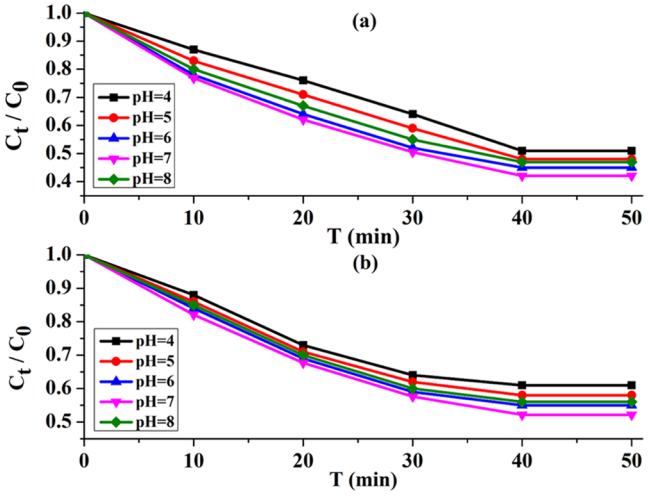

Figure 5. Effect of pH on the adsorption of (a) Cr(VI) and (b) Mn(VII).

X-ray powder diffraction (Figure S5) showed that the diffraction peaks of **1** adsorbed with Cr(VI) and Mn(VII) overlapped well with the theoretical simulated diffraction peaks. This shows that the structure of **1** has not changed after the adsorption of Cr(VI) and Mn(VII). Therefore, the cyclic experiment of **1** was explored in the solution of 25 °C and pH 7.

https://doi.org/10.1021/acsomega.3c04177
ACS Omega 2023, 8, 36978−36985

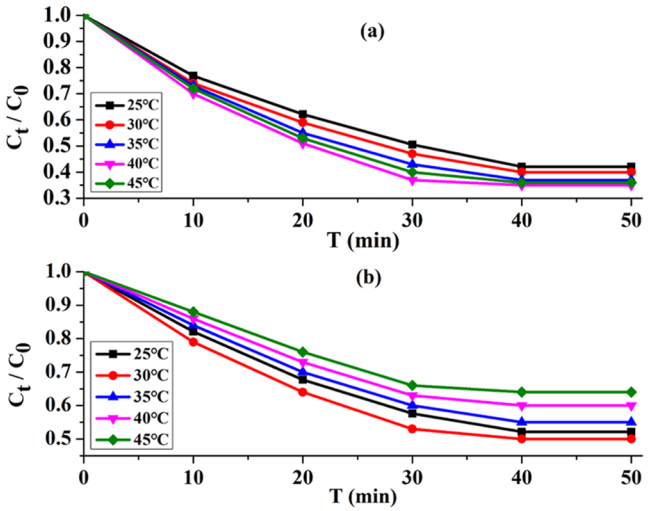

Figure 6. Effect of temperature on **1** adsorption of (a) Cr(VI) and (b) Mn(VII).

The cyclic experiment results (Figure 7) showed that **1** had good cyclic regeneration and adsorption efficiency. The equilibrium

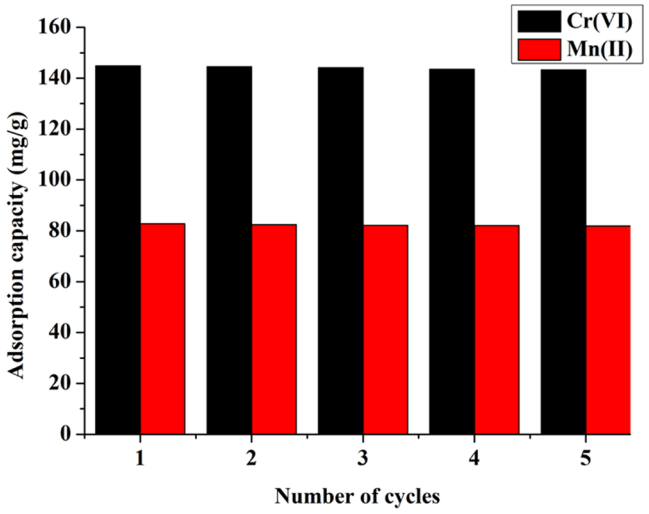

Figure 7. Cycle experiment of **1**.

adsorption amounts of Cr(VI) adsorbed by **1** for five cycles are 144.8 144.5, 144.1, 143.5, and 143.2 mg/g, respectively. It can be seen that the adsorption efficiency of **1** remains at 98.76% after five cycles. Similarly, the equilibrium adsorption amounts of Mn(VII) adsorbed by **1** for five times are 82.75 82.43, 82.18, 82.03, and 81.91 mg/g, respectively. It can be seen that the adsorption efficiency of **1** remains at 98.69% after five cycles. The above cyclic adsorption results of Cr(VI) and Mn(VII) show that **1** has good cyclic regeneration and adsorption properties. It has the potential to adsorb high-valence heavy metal ions in industrial wastewater.

4. CONCLUSIONS

In summary, a two-dimensional copper-based metal−organic framework, $\{[Cu\cdot(4,4'\text{-bpy})_2\cdot(H_2O)]\cdot 2(NO_3)\cdot 6(H_2O)\cdot(CH_3OH)\}_n$ (**1**), is successfully synthesized by hydrothermal synthesis. The structure of **1** is characterized by infrared (IR) spectroscopy, elemental analysis, X-ray photoelectron spectroscopy (XPS), and single-crystal X-ray diffraction. The results show that **1** is an inorganic coordination polymer, which is composed of $[Cu\cdot(4,4'\text{-bpy})_2\cdot(H_2O)]^{2+}$ and NO_3^-. It has good adsorption performance of Cr(VI) and Mn(VII) in the pH range 4−8. The adsorption performance is the best when pH is 7, which can reach 145 and 83 mg/g, respectively. Moreover, after five adsorption cycles of Cr(VI) and Mn(VII), the adsorption efficiency remained at 98.76 and 98.69%, respectively. It has the potential to adsorb high-valence heavy metal ions in industrial wastewater.

■ ASSOCIATED CONTENT

Supporting Information

The Supporting Information is available free of charge at https://pubs.acs.org/doi/10.1021/acsomega.3c04177.

data_7-26 (CIF)
7-26_sq-Revised (CIF)
IR of 4,4′- bpy and **1**; N_2 adsorption/desorption isotherm of **1**; pore size distribution of nanomaterial; TGA of **1**; XRD of 1 after desorption (Figures S1−S5); crystal parameters of **1**; partial bond length (nm) and bond angle (°) of **1** (Tables S1−S2) (PDF)

■ AUTHOR INFORMATION

Corresponding Author

Shixiong Li − *School of Mechanical and Resource Engineering, Wuzhou University, Wuzhou, Guangxi 543002, China; Wuzhou Resource Recycling Engineering Technology Research Center, Wuzhou University, Wuzhou, Guangxi 543002, China;* orcid.org/0000-0002-6600-1749; Email: lsx1324@163.com

Authors

Yongmou Zeng − *School of Mechanical and Resource Engineering, Wuzhou University, Wuzhou, Guangxi 543002, China*

Xia Li − *School of Mechanical and Resource Engineering, Wuzhou University, Wuzhou, Guangxi 543002, China*

Yuhuan Chen − *School of Mechanical and Resource Engineering, Wuzhou University, Wuzhou, Guangxi 543002, China*

Complete contact information is available at: https://pubs.acs.org/10.1021/acsomega.3c04177

Author Contributions

S.L. designed and conceived the experiments, and wrote the paper; X.L. performed the synthesis of **1**; Y.Z. did an organic pollutant degradation experiment and analyzed the structure of **1**. Y.C. analyzed the concentration of pollutants. All authors participated in the analysis, interpretation, and review of the results and provided input in the writing process of the paper.

Notes

The authors declare no competing financial interest.

■ ACKNOWLEDGMENTS

This work was supported by the industry, academia, and research projects in Wuzhou High-tech Industrial Development Zone and Wuzhou University (no. 2020G011); Guangxi Natural Science Foundation, China (no. AD23026019); Guangxi University Young and Middle-aged Teachers' Basic Scientific Research Ability Improvement Project (no. 2023KY0710); and Wuzhou University Research Foundation for Advanced Talents (no. WZUQDJJ21081).

REFERENCES

(1) Li, S.; Luo, P.; Wu, H.; Wei, C.; Hu, Y.; Qiu, G. Strategies for Improving the Performance and Application of MOFs Photocatalysts. *ChemCatChem.* **2019**, *11* (13), 2978−2993.

(2) Li, D.; Liu, J.; Wang, S.; Cheng, J. Study on coal water slurries prepared from coal chemical wastewater and their industrial application. *Appl. Energy* **2020**, *268*, No. 114976.

(3) Li, S.; Fen, Z.; Hu, Y.; Wei, C.; Wu, H.; Huang, J. In-Situ Synthesis and High-Efficiency Photocatalytic Performance of Cu(I)/Cu(II) Inorganic Coordination Polymer Quantum Sheets. *Inorg. Chem.* **2018**, *57* (21), 13289−13295.

(4) Ahmad, A.; Banat, F.; Alsafar, H.; Hasan, S. W. Algae biotechnology for industrial wastewater treatment, bioenergy production, and high-value bioproducts. *Sci. Total Environ.* **2022**, *806*, No. 150585.

(5) Chen, X.; Song, Z.; Yuan, B.; Li, X.; Li, S.; Thang Nguyen, T.; Nguyen, T. T.; Guo, Z. Fluorescent carbon dots crosslinked cellulose Nanofibril/Chitosan interpenetrating hydrogel system for sensitive detection and efficient adsorption of Cu (II) and Cr (VI). *Chem. Eng. J.* **2022**, *430*, No. 133154.

(6) Chen, B.; Li, L.; Liu, L.; Cao, J. Effective adsorption of heavy metal ions in water by sulfhydryl modified nano titanium dioxide. *Front. Chem.* **2023**, *10*, No. 1072139.

(7) Arslan, H.; Eskikaya, O.; Bilici, Z.; Dizge, N.; Balakrishnan, D. Comparison of Cr (VI) adsorption and photocatalytic reduction efficiency using leonardite powder. *Chemosphere* **2022**, *300*, No. 134492.

(8) Stern, C. M.; Jegede, T. O.; Hulse, V. A.; Elgrishi, N. Electrochemical reduction of Cr(VI) in water: lessons learned from fundamental studies and applications. *Chem. Soc. Rev.* **2021**, *50* (3), 1642−1667.

(9) Shi-Xiong, L.; An-Qi, F.; Yuan, H.; Gui-Chun, L.; Li-Fei, L.; Hui-Ping, L. Two-Dimensional Copper-Based Coordination Polymer: Synthesis, Structure and Ion Effect on Adsorption of Cr(VI). *Chin. J. Inorg. Chem.* **2022**, *38* (5), 941−950.

(10) Yang, S.; Chen, Y.; Li, S. In-situ Synthesis Mechanism and High-efficiency Photocatalytic Activity of Black Cu(I)/Cu(II) Ultrathin Nanosheets. *Inorg. Chim. Acta* **2023**, *556*, No. 121660.

(11) Qi, X.; Tong, X.; Pan, W.; Zeng, Q.; You, S.; Shen, J. Recent advances in polysaccharide-based adsorbents for wastewater treatment. *J. Cleaner Prod.* **2021**, *315*, No. 128221.

(12) Solangi, N. H.; Kumar, J.; Mazari, S. A.; Ahmed, S.; Fatima, N.; Mubarak, N. M. Development of fruit waste derived bio-adsorbents for wastewater treatment: A review. *J. Hazard. Mater.* **2021**, *416*, No. 125848.

(13) Barszcz, B.; Masternak, J.; Kowalik, M. Structural insights into coordination polymers based on 6s2 Pb (II) and Bi (III) centres connected via heteroaromatic carboxylate linkers and their potential applications. *Coord. Chem. Rev.* **2021**, *443*, No. 213935.

(14) Zhao, J. J.; Liu, P. Y.; Song, L. J.; Zhang, L.; Liu, Z. L.; Wang, Y. Q. A water stable Eu (III)−organic framework as a recyclable multi-responsive luminescent sensor for efficient detection of p-aminophenol in simulated urine, and Mn(VII) and Cr(VI) anions in aqueous solutions. *Dalton Trans.* **2021**, *50* (15), 5236−5243.

(15) Babapour, M.; Dehghani, M. H.; Alimohammadi, M.; Arjmand, M. M.; Salari, M.; Rasuli, L.; Mubarak, N. M.; Khan, N. A. Adsorption of Cr(VI) from aqueous solution using mesoporous metal-organic framework-5 functionalized with the amino acids: Characterization, optimization, linear and nonlinear kinetic models. *J. Mol. Liq.* **2022**, *345*, No. 117835.

(16) Wang, C.; Xiong, C.; He, Y.; Yang, C.; Li, X.; Zheng, J.; Wang, S. Facile preparation of magnetic Zr-MOF for adsorption of Pb (II) and Cr (VI) from water: Adsorption characteristics and mechanisms. *Chem. Eng. J.* **2021**, *415*, No. 128923.

(17) Li, J. X.; Du, Z. X.; Pan, Q. Y.; Zhang, L. L.; Liu, D. L. The First 3, 5, 6-trichloropyridine-2-oxyacetate Bridged Manganese Coordination Polymer with Features of $\pi\cdots\pi$ Stacking and Halogen···Halogen Interactions: Synthesis, Crystal Analysis and Magnetic Properties. *Inorg. Chim. Acta* **2020**, *509*, No. 119677.

(18) Li, J. X.; Du, Z. X. A binuclear cadmium(II) Cluster Based on $\pi\cdots\pi$ Stacking and Halogen··· Halogen Interactions: Synthesis, Crystal analysis and Fluorescent Properties. *J. Clust. Sci.* **2020**, *31* (2), 507−511.

(19) Li, S. X.; Huang, F. L.; Bin, Y. J.; Wei, Y. C.; Tang, X. L.; Liao, B. L. Effect of Ions on Photocatalytic Performance of UIO-66−2OH. *Chin. J. Inorg. Chem.* **2021**, *37*, 1465−1474.

(20) Liao, B.; Li, S. Multifunctional Mn(II) Metal-Organic framework for photocatalytic aerobic oxidation and C-H direct trifluoromethylation. *J. Catal.* **2022**, *414*, 294−301.

(21) Li, J. X.; Xiong, L. Y.; Fu, L. L.; Bo, W. B.; Du, Z. X.; Feng, X. Structural diversity of Mn(II) and Cu(II) complexes based on 2-carboxyphenoxyacetate linker: Syntheses, conformation comparison and magnetic properties. *J. Solid State Chem.* **2022**, *305*, No. 122636.

(22) Azhar, M. R.; Abid, H. R.; Sun, H.; Periasamy, V.; Tadé, M. O.; Wang, S. Excellent performance of copper based metal organic framework in adsorptive removal of toxic sulfonamide antibiotics from wastewater. *J. Colloid Interface Sci.* **2016**, *478*, 344−352.

(23) Haso, H. W.; Dubale, A. A.; Chimdesa, M. A.; Atlabachew, M. High performance copper based metal organic framework for removal of heavy metals from wastewater. *Front. Mater.* **2022**, *9*, No. 840806.

(24) Eliwa, A. S.; Ali, A. E.; Hosny, W. M.; Mohamed, G. G.; Deghadi, R. G. Sonochemical synthesis and characterization of novel copper based metal-organic framework: Its application as electrochemical sensor for determination of Cd(II) ion in real water samples. *Inorg. Chem. Commun.* **2023**, *153*, No. 110733.

(25) Dolomanov, O. V.; Bourhis, L. J.; Gildea, R. J.; Howard, J. A.; Puschmann, H. OLEX2: a complete structure solution, refinement and analysis program. *J. Appl. Crystallogr.* **2009**, *42* (2), 339−341.

(26) Ru-Xia, L.; Wen-Bin, Z.; Lin-Hua, X.; Ya-Bo, X.; Jian-Rong, L. Recent Advances in Adsorptive Removal of Cr(VI) Ions by Metal-Organic Frameworks. *Chin. J. Inorg. Chem.* **2021**, *37*, 385−400.

(27) Jamshidifard, S.; Koushkbaghi, S.; Hosseini, S.; Rezaei, S.; Karamipour, A.; Rad, J. A.; Irani, M. Incorporation of UiO-66-NH_2 MOF into the PAN/chitosan Nanofibers for Adsorption and Membrane Filtration of Pb(II), Cd(II) and Cr(VI) Ions from Aqueous Solutions. *J. Hazard. Mater.* **2019**, *368*, 10−20.

https://doi.org/10.1021/acsomega.3c04177
ACS Omega 2023, 8, 36978−36985